Lanthanide-Based Lamellar Nanohybrids: Synthesis, Structural Characterization, and Optical Properties

Mohamed Karmaoui,[†,‡] Rute A. Sá Ferreira,[§] Ankush T. Mane,[†] Luís D. Carlos,[§] and Nicola Pinna*[,†,‡,||]

Institut für Anorganische Chemie, Martin-Luther-Universität Halle-Wittenberg, Kurt-Mothes-Strasse 2, 06120 Halle (Saale), Germany, Departamentos de Química e Física, CICECO, Universidade de Aveiro, 3810-193 Aveiro, Portugal, and Max Planck Institute of Microstructure Physics, Weinberg 2, D-06120 Halle (Saale), Germany

Received March 23, 2006. Revised Manuscript Received June 23, 2006

A general nonaqueous route has been applied for the preparation of lanthanide ordered nanocrystalline hybrid structures. In a simple one-pot reaction process, Ln(III) isopropoxides (Ln = Gd, Sm, Nd) were dissolved in benzyl alcohol and reacted in an autoclave between 250 and 300 °C. This approach leads to crystalline lanthanide oxide layers regularly separated from each other by organic layers of intercalated benzoate molecules. They display good thermal stability for temperature up to 400 °C. The gadolinium-based nanohybrids showed outstanding optical emission properties when doped with terbium(III) and europium(III).

Introduction

Rare earth metal oxides have wide applications in today's life. Their intrinsic dielectric properties make them good candidates for multilayered capacitors, ferroelectric memories, or complementary metal oxide semiconductor- (CMOS-) based devices.[1,2] Because of their thermal stability and surface reactivity, they find applications in heterogeneous catalysis.[3] However they are mostly known for their emission properties; in fact lanthanides show intense emission under UV excitation when diluted in an appropriate host network (mostly other rare earth oxides such as yttrium, lanthanum, or gadolinium).[4] Such emission can be tuned simply by changing the rare earth cation. Indeed, one can find those phosphors in our televisions, luminescent lamps, or flat screens.

At the nanoscale, rare earth oxides show improved properties, for example, enhanced catalytic properties because of their larger surface available, or new application fields such as luminescent biological labels. Few examples of chemical synthesis of rare earth nanoparticles have been recently published. In the majority of the cases, to form the pure oxide phase, a thermal treatment is needed after precipitation of hydroxide precursors;[5,6] hence, the powders synthesized in this way are characterized by large polydispersity and uncontrolled particle shape. Only a few examples of direct formation of rare earth oxide nanoparticles have been published[7,8] and their optical properties studied.[9]

Ordered organic/inorganic hybrids are multifunctional materials offering a large variety of physical properties;[10] in fact, they depend not only on both the inorganic and organic components but also on the interface between the two phases.[11] Furthermore, the organic component can be easily modified in order to precisely tune the global properties of the final material. Many examples of such ordered nanohybrids exist in the literature and were well summarized in some reviews of Sanchez and co-workers.[10,11] For example, the incorporation of a wide range of chemical species in vanadium pentoxide xerogels was studied;[12] or vanadium oxide nanotubes (VO_x NTs) were synthesized by a sol−gel reaction of a vanadium(V) alkoxide or vanadium pentoxide with a primary amine or a $\alpha-\omega$-diamine, followed by hydrothermal treatment.[13,14]

In the past few years it has been shown that nonaqueous sol−gel reactions of benzyl alcohol with different metal oxide precursors (alkoxides, chlorides, acetylacetonates, etc.) allow

* Corresponding author: e-mail pinna@ciceco.ua.pt; fax +351 234370004.
† Martin-Luther-Universität Halle-Wittenberg.
‡ Departamento de Química, CICECO, Universidade de Aveiro.
§ Departamento de Física, CICECO, Universidade de Aveiro.
|| Max Planck Institute of Microstructure Physics.

(1) Jones, A. C.; Aspinall, H. C.; Chalker, P. R.; Potter, R. J.; Kikli, K.; Rahtu, A.; Ritala, M.; Leskelä, M. *J. Mater. Chem.* **2004**, *14*, 3101.
(2) Leskalä, M.; Ritala, M. *J. Solid State Chem.* **2003**, *171*, 170
(3) Cuif, J.-P.; Rohart, E.; Macaudiere, P.; Bauregard, C.; Suda, E.; Pacaud, B.; Imanaka, N.; Masui, T.; Tamura, S. *Binary Rare Earth Oxides*; Adachi, G., Imanaka, N., Kang, Z. C., Eds.; Kluwer Academic Publishers: Dordrecht, The Netherlands, 2004; p 215
(4) Blasse, G.; Grabmaier, B. C. *Luminescent Materials*; Springer: Berlin, 1994.
(5) Feldmann, C. *Adv. Funct. Mater.* **2003**, *13*, 101.
(6) Kepinski, L.; Zawadzke, M.; Mista, W. *Solid State Sci.* **2004**, *6*, 1327.
(7) (a) Huignard, A.; Gacoin, T.; Boilot, J.-P. *Chem. Mater.* **2000**, *12*, 1090. (b) Bazzi, R.; Flores, M. A.; Louis, C.; Lebbou, K.; Zhang, W.; Dujardin, C.; Roux, S.; Mercier, B.; Ledoux, G.; Bernstein, E.; Perriat, P.; Tillement, O. *J. Colloid Interface Sci.* **2004**, *273*, 191.
(8) (a) Cao, Y. C. *J. Am. Chem. Soc.* **2004**, *126*, 7456. (b) Si, R.; Zhang, Y.-W.; You, L.-P.; Yan, C. H. *Angew. Chem., Int. Ed.* **2005**, *44*, 3256.
(9) Bazzi, R.; Flores-Gonzalez, M. A.; Louis, C.; Lebbou, K.; Dujardin, C.; Brenier, A.; Zhang, W.; Tillement, O.; Bernstein, E.; Perriat, P. *J. Lumin.* **2003**, *102*−*103*, 445.
(10) Sanchez, C.; Ribot, F. *New J. Chem.* **1994**, *18*, 1007.
(11) Sanchez, C.; Lebeau, B.; Chaput, F.; Boilot, J.-P. *Adv. Mater.* **2003**, *15*, 1969.
(12) Livage, J. *Chem. Mater.* **1991**, *3*, 578.
(13) Krumeich, F.; Muhr, H. J.; Niederberger, M.; Bieri, F.; Schnyder, B.; Nesper, R. *J. Am. Chem. Soc.* **1999**, *121*, 8324.
(14) Niederberger, M.; Muhr, H.J.; Krumeich, F.; Bieri, F.; Günther, D.; Nesper, R. *Chem. Mater.* **2000**, *12*, 1995.

10.1021/cm060705l CCC: $33.50
Published on Web 08/04/2006

the controlled and straightforward synthesis of various crystalline metal oxide nanoparticles.[15] In one "exceptional" case it was found that the reaction of benzyl alcohol with yttrium(III) isopropoxide leads to an unusual ordered hybrid nanostructured material that consists of very thin layers of yttrium oxide (~0.6 nm) regularly separated from each other by organic layers of intercalated benzoate molecules.[16] From the study of the formation mechanism, it was found that a Cannizzaro-like reaction forming the benzoate species, catalyzed by the newly formed yttrium oxide, takes place at its surface, blocking further grow and thus forming the hybrid structure. The ability to catalyze this Cannizzaro-like reaction is the key to the formation of the ordered nanohybrid structure. In the present work we prove that similar reactions take place at the surface of lanthanide oxides and lead to the formation of similar nanohybrids characterized by nearly identical structural and thermal stability properties. Finally, the outstanding optical properties in the visible region of the gadolinium-based nanohybrids doped with Eu(III) and Tb(III) and in the infrared region of neodymium-based nanohybrids are investigated.

Experimental Details

The synthesis procedures were carried out in a glovebox (O_2 and H_2O < 0.1 ppm). In a typical synthesis of the nanohybrids, yttrium(III) isopropoxide [Strem; $Y_5O(OC_3H_7)_{13}$; 500 mg, 0.407 mmol], neodymium(III) isopropoxide [Strem; $Nd(OC_3H_7)_3$; 400 mg, 1.244 mmol], samarium(III) isopropoxide [Strem; $Sm_5O(OC_3H_7)_{13}$; 400 mg, 0.260 mmol], or gadolinium(III) isopropoxide [synthesized following published method;[17] 200 mg of $Gd(OC_3H_7)_3$ 0.598 mmol) was added to anhydrous benzyl alcohol (Aldrich; 20 mL, 193 mmol; or 15 mL, 145 mmol in the case of gadolinium). In the case of the Eu(III)- and Tb(III)-doped nanocomposites, 5 mol % lanthanide-(III) isopropoxide was replaced by anhydrous europium(III) or terbium(III) chloride. The reaction mixture was transferred into a Teflon cup of 45 mL inner volume, slid into a steel autoclave, and carefully sealed (reaction temperature 250 °C). For higher temperature reactions, a glass beaker was used instead of the Teflon cup. The autoclave was taken out of the glovebox and heated in a furnace at 250 or 300 °C for 2 days. The resulting milky suspensions were centrifuged, and the precipitates were thoroughly washed with ethanol and dichloromethane and subsequently dried in air at 80 °C.

Carbon, hydrogen, and nitrogen elemental analysis (CHN) and atomic absorption elemental analysis were performed in order to determine the stoichiometry of the different samples and the Tb and Eu doping efficiency. CHN results are shown in the Supporting Information. The determined ratios Tb/Gd = 0.033 and Eu/Gd = 0.037 were only slightly lower than the nominal value of (Eu,Tb)/Gd = 0.050, demonstrating good doping efficiency.

The X-ray powder diffraction (XRD) diagrams of all samples were measured in transmission mode (Co Kα radiation) on a STOE STADI MP equipped with IP-PSD image plate detector.

For TEM measurements, one or more drops of the solution of nanohybrids in ethanol were deposited on the amorphous carbon film. A Philips CM20 microscope operating at 200 kV was used.

Fourier transform infrared spectroscopy (FT-IR, Mattson 5000) was carried out in the range of 4000−450 cm^{-1} in transmission mode. The pellets were prepared by adding 1−2 mg of the nanohybrid powder to 200 mg of KBr. The mixture was then carefully mixed and compressed at a pressure of 10 kPa in order to form transparent pellets.

For evaluation of the formation mechanism, the reaction solution obtained by centrifugation of the solid material was subjected to NMR analysis on a Varian Inova 500 MHz instrument at room temperature.

The thermal behavior of the nanopowders was investigated with a thermoanalyzer (Netzsch STA 409C/CD) apparatus. All samples were recorded at a scan rate of 10 °C min^{-1} from room temperature to 800 °C under air or argon atmosphere.

The emission and excitation spectra were recorded between 14 and 300 K on a modular double-grating excitation spectrofluorometer with a Triax 320 emission monochromator (Fluorolog-3, Jobin Yvon-Spex) coupled to a R928 Hamamatsu photomultiplier. The excitation source was a 450 W Xe arc lamp. All the spectra, corrected for optics and detection spectral response, were measured in the front-face acquisition mode. Photoluminescence quantum yield measurements were performed with the setup described above. The near-IR emission was recorded on a Brüker RFS100/S FT spectrometer (Nd:YAG laser excitation, 1064 nm). The lifetime measurements were acquired with the setup described for the luminescence spectra by use of a pulsed Xe−Hg lamp (6 μs pulse at half width and 20−30 μs tail).

The absolute emission quantum yields (φ) were measured at room temperature via the technique for powder samples described by Brilland De Jager-Veenis,[18] through the following expression:

$$\phi = \left(\frac{1 - r_{st}}{1 - r_x}\right)\left(\frac{A_x}{A_{st}}\right)\phi_{st}$$

where r_{st} and r_x are the diffuse reflectance (with respect to a fixed wavelength) of the standard phosphor and of the hybrid, respectively, and ϕ_{st} is the quantum yield of the standard phosphor. The terms A_x and A_{st} represent the area under the hybrid and the standard phosphor emission spectra, respectively. Diffuse reflectance and emission spectra were acquired with the experimental setup aforementioned to detect photoluminescence. To have absolute intensity values, $BaSO_4$ was used as reflecting standard (r = 91%). The same experimental conditions, namely, position of the hybrids/standard holder, excitation and detection monochromator slits (0.3 mm), and optical alignment, were fixed. To prevent insufficient absorption of the exciting radiation, a powder layer around 3 mm was used and utmost care was taken in order to ensure that only the sample was illuminated, to diminish the quantity of light scattered by the front sample holder. The standard phosphor used was sodium salicylate (Merck P.A.), whose emission spectra are formed by a large broad band peaking around 425 nm, with a constant ϕ value (60%) for excitation wavelengths between 220 and 380 nm. Four measurements were carried out, so that the presented ϕ value corresponds to the arithmetic mean value. The errors in the quantum yield values associated with this technique were estimated within 10%.[18]

Results and Discussion

Structural Characterization. The reaction of lanthanide isopropoxides in benzyl alcohol results in the direct formation

(15) (a) Niederberger, M.; Bartl, M. H.; Stucky, G. D. *J. Am. Chem. Soc.* **2002**, *124*, 13642. (b) Pinna, N.; Garnweitner, G.; Antonietti, M.; Niederberger, M. *Adv. Mater.* **2004**, *16*, 2196. (c) Niederberger, M.; Pinna, N.; Polleux, J.; Antonietti, M. *Angew. Chem., Int. Ed.* **2004**, *43*, 2270. (d) Pinna, N.; Neri, G.; Antonietti, M.; Niederberger, M. *Angew. Chem., Int. Ed.* **2004**, *43*, 4345. (e) Pinna, N.; Grancharov, S.; Beato, P.; Bonville, P.; Antonietti, M.; Niederberger, M. *Chem. Mater.* **2005**, *17*, 3044. (f) Pinna, N.; Antonietti, M.; Niederberger, M. *Colloids Surf., A* **2004**, *250*, 211.

(16) Pinna, N.; Garnweitner, G.; Beato, P.; Niederberger, M.; Antonietti, M. *Small* **2005**, *1*, 112.

(17) Mehrotra, R. C.; Batwara, J. M. *Inorg. Chem.* **1970**, *9*, 2505.

(18) Brill, A.; De Jager-Veenis, A. W. *J. Electrochem. Soc.* **1976**, *123*, 396.

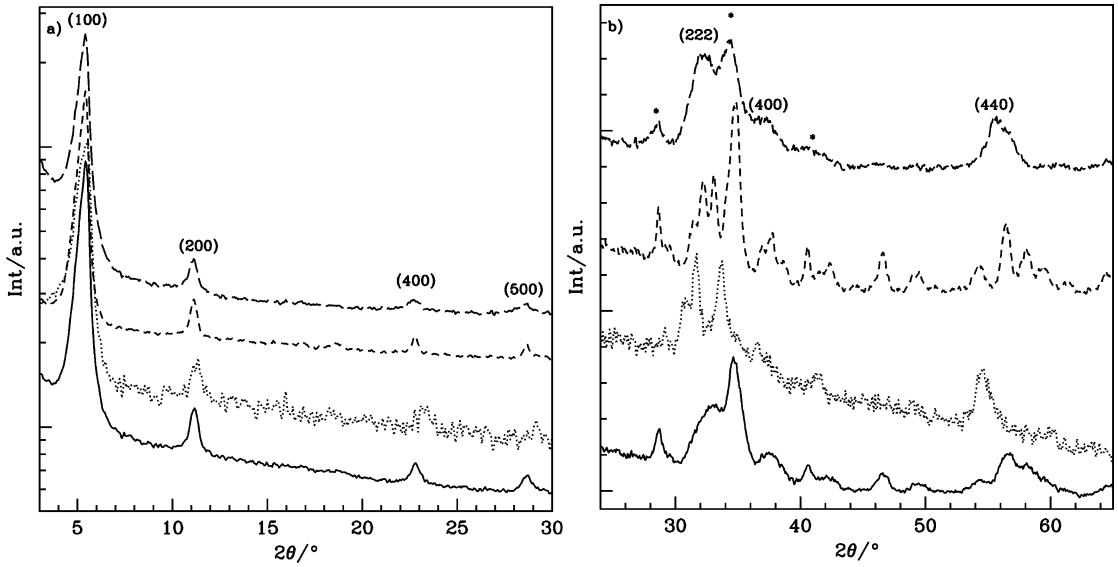

Figure 1. XRD patterns of the nanohybrids samples: yttrium- (—), neodymium- (•••), samarium- (---) (synthesized at 300 °C), and gadolinium- (— — —) based nanohybrids. (a) Small-angle region; (b) wide-angle region in which the reflections due to the mesostructure are indicated by asterisks.

of lamellar inorganic−organic nanohybrids based on Ln_2O_3-type oxides. At the end of the reaction, for each lanthanide precursor, thin crystalline powders, white (in the case of gadolinium or yttrium),[19] light yellow (samarium), or pale blue (neodymium), are obtained.

X-ray diffraction provides complex patterns containing full information about the mesostructural order and the crystalline one; for this reason a detailed study is needed.

Figure 1a shows the low-angle part of the diffraction patterns ($4° < 2\theta < 30°$) where the reflections observed are due to the mesocrystalline order. The first most intense peak observed for a diffraction angle (2θ for the cobalt radiation) of around 5.5° corresponds to a distance of 1.8 nm, hence to the 100 reflection of the lamellar structure. The higher orders up to the fifth could be clearly assigned on the same figure. Even higher orders are visible on the wide-angle part of the pattern (Figure 1b), especially the sixth at $2\theta \sim 35°$, which is as intense and overlaps with the near reflections due to the crystalline inorganic layers (zone $30° < 2\theta < 40°$). The extinction of the third order is typical for lamellar structure where the thickness of one layer is double that of the other. This is exactly what happens in our system where the inorganic layer is twice as thin as the organic one. This high number of reflections, due to the lamellar periodicity, denotes the high order and the monodispersity in term of organic and inorganic layer thicknesses. Surprisingly, the position of these reflections is the same for each sample. Hence, the thickness of the inorganic and organic layers is constant and does not vary with regard to the nature of the oxide.

Information regarding the crystal structure of the inorganic layer is found mainly in the regions $30° < 2\theta < 40°$ and $2\theta \sim 55°$ (Figure 1b). Each oxide is characterized by a first broad peak $2\theta \sim 33°$, which could correspond to the 222 reflection of the cubic structure of these Ln_2O_3-type oxides (JCPDS: Y_2O_3 41-1105, Nd_2O_3 21-579, Sm_2O_3 15-813, and Gd_2O_3 43-1014), a second broad peak around $2\theta \sim 37°$ that could be attributed to the 400 reflection, and a last main broad reflection ($2\theta \sim 56°$) attributed to the 440. However, the shape of the 222 reflection is not always symmetric or presents a splitting, which could denote that in fact the structure is not cubic but monoclinic (JCPDS: Y_2O_3 44-399, Nd_2O_3 28-671, Sm_2O_3 42-1464, and Gd_2O_3 43-1015). This hypothesis is difficult to demonstrate by XRD or other diffraction techniques, in fact, since the inorganic layers are extremely thin (~0.6 nm) the diffractions observed are broad and do not permit a clear identification. Furthermore, in the same 2θ region there is the sixth order of the mesotructure ($2\theta \sim 35°$) that overlaps with the diffractions of the inorganic layers. To make the text more readable, from now on we will use the Miller indices of cubic structure to refer to the diffractions of the inorganic layers.

Figure 2 panels a and d show transmission electron microscopy (TEM) studies of neodymium and gadolinium nanohybrids, respectively. Similar to the case of the yttrium,[16] the samples consist of a lamellar structure oriented in the same direction. The oxidic part (i.e., the one that scatters strongly the incident electrons) is seen as dark layers. In contrast, the organic material stays practically invisible between those layers.

The Fourier transforms of these images (Figure 2b,e) give rise to pairs of spots that can be attributed to the reflections of the mesostructure. Their selected area electron diffractions (SAED) are more complex to analyze but contain information on the mesostructure, crystal structure and growth orientation of the inorganic layers (Figure 2c,f). The series of spots at low angle (indicated by an ellipsoid) are the ones due to the scattering of the lamellar structure. The first order is nearly totally enclosed in the incident beam and almost not visible. The high lamellar order is again proved by the many orders of the reflections present (up to seven in the case of neodymium, Figure 2c). In the same SAED, perpendicular to the lamellar order, some broad spots noted as 222 and 440 are present. They are responsible for the diffraction of

(19) Even though the yttrium-based nanohybrid was already studied,[16] it is presented in the text as comparison due to its structural similarities with the lanthanide cases.

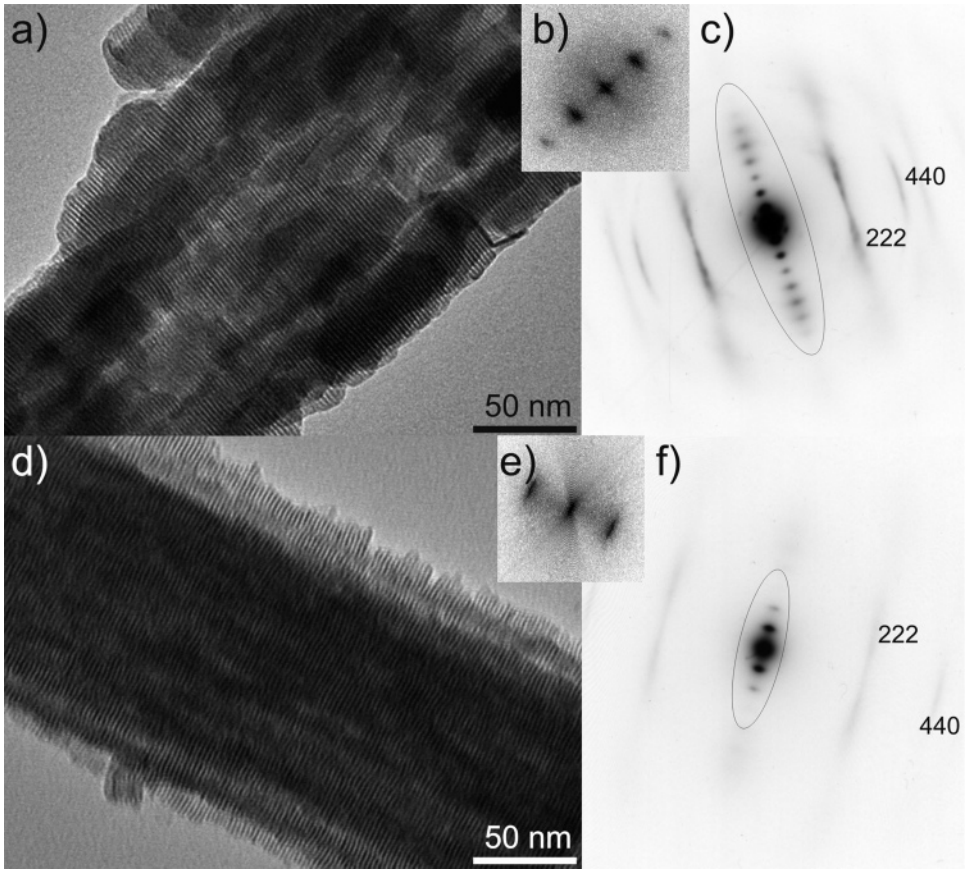

Figure 2. TEM images of the neodymium- (a) and gadolinium- (d) based nanohybrids synthesized at 250 °C. Their respective Fourier transforms (b and e), and their SAED (c and f) are also shown.

the inorganic layers. From the angle between those reflections and since the 440 is exactly perpendicular to the lamellar order, it is deduced that the main facets exposed of the inorganic layers are the {001}.

The case of samarium is slightly different (Figure 3); in fact, for a synthesis at 250 °C it shows mainly very thin (<2 nm) monocrystalline Sm_2O_3 platelets (Figure 3a) and at the same time some lamellar nanohybrids, as is the case for the other rare earth examples (Figure 3b). The platelets formed at this temperature have a tendency to stack, but many free platelets were also observed. To achieve a high-quality nanohybrid, as in the case of yttrium, gadolinium, or neodymium, the reaction temperature had to be increased to 300 °C (Figure 3c). In this case the obtained organic/inorganic hybrid is formed of nanoparticles that are ~25 nm in width and 50−80 nm in length. Each particle shows well-defined lamellar structure. The SAED of such a zone (Figure 3d) presents many rings containing information about the high lamellar order; in fact, up to seven orders are present. Few additional rings are due to the diffraction of the inorganic part. To avoid confusion with the ones due to the mesostructure, on the figure they are noted with the usual Miller indices in black boxes. In the case of samarium, rings instead of spots are observed because the nanohybrid particles are oriented randomly on the carbon film. The reason for the slightly different behavior of the samarium-based nanohybrid is not known yet, but it could be due to a higher stability of the precursor alkoxide or to a higher temperature required by the samarium in order to catalyze the Cannizzaro reaction that leads to the benzoate complex formation (see below).

The temperature stability of the nanohybrids was studied by thermogravimetric analysis (TGA) coupled with differential thermal analysis (DTA) under air. Figure S1 (Supporting Information) shows the results for each sample. They show the same global behavior: before 400 °C the weight loss is principally due to molecules adsorbed at the surface, like benzyl alcohol, which is known to start to desorb at around 150 °C.[20] In fact, no peak in the DTA is observed between 150 and 400 °C. The main weight loss takes place between 400 and 500 °C; it is accompanied by a sharp exothermic peak in the DTA, which is attributed to the combustion of the intercalated organic molecules. At higher temperature the recrystallization and growth takes place. Once more the nanohybrid structures show, as already seen by XRD and TEM studies, similar characteristics and behavior. It is surprising that those hybrid structures that are built up only because of $\pi-\pi$ interactions (see below) are stable at temperature as high as 400 °C.

The nature of the organic layer forming the yttrium oxide nanohybrid was extensively studied in our previous article[16] by vibrational spectroscopy and ^1H and ^{13}C solid-state NMR.

Briefly, it was found that benzoate species forming a bridge-like bond with the yttria layer were the only species present between the inorganic layer, and thus they were responsible of the formation of the nanohybrid structure. Furthermore, the reaction mixture was carefully investigated after synthesis in order to understand how the benzoate

(20) Niederberger, M.; Bartl, M. H.; Stucky, G. D. *Chem. Mater.* **2002**, *14*, 4364.

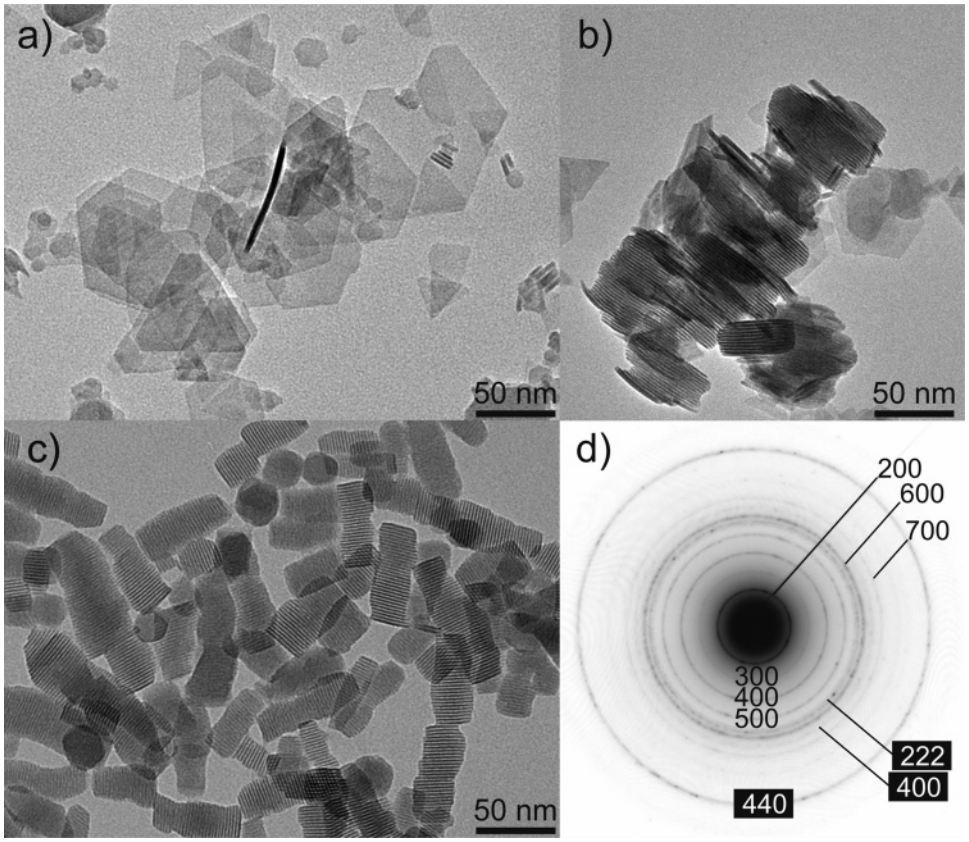

Figure 3. TEM images of the samarium nanohybrid synthesized at 250 °C (a, b) and at 300 °C (c). (d) SAED of the sample in panel c, where the Miller indices of the lamellar order (unboxed numbers) and crystal structure (black boxed numbers) are shown.

species could be formed and why they could control so precisely the growth, and thus the thickness, of the inorganic layer. We proposed that a hydride transfer reaction catalyzed by the yttrium oxide nanostructure is responsible for the formation of benzoate molecules directly coordinated to the metal centers. A critical size/thickness of the yttria layer is the condition required for such a catalyzed reaction. From the structural characterization presented above, it seems that the same reaction is taking place also in the case of the lanthanide samples studied in the present work. Hence, the neodymium, samarium, and gadolinium oxide thin layers could catalyze the Cannizzaro-like reaction responsible for the formation of benzoate species.[16,21] Therefore, similar characterization techniques were used in this present work in order to prove this hypothesis. First of all, FT-IR spectra of each nanohybrid were acquired and compared (see Supporting Information, Figure S4). The obtained spectra are very similar. The region between 1700 and 1300 cm^{-1} (i.e., the region characteristic of the symmetric and asymmetric carboxylic stretching frequencies) could be nearly superposed, proving that indeed only benzoate species form the organic layers. The typical signature of oxidic bonds is present in the small-wavenumber region ($\sim$600 cm^{-1} and below). Second, the reaction mixtures were studied by ^{13}C and ^{1}H NMR and the same organic species as in the case of the yttrium were found, proving that in fact the formation of the nanohybrid structures follows the same reaction scheme.

(21) Haffad, D.; Kameswari, U.; Bettahar, M. M.; Chambellan, A.; Lavalley, J. C. *J. Catal.* **1997**, *172*, 85.

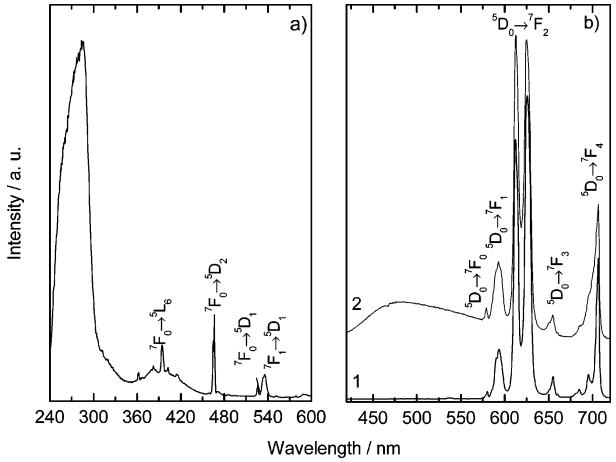

Figure 4. Room-temperature (a) excitation and (b) emission spectra of gadolinium/europium-based nanohybrid monitored around 625 nm excited at (1) 285 and (2) 395 nm, respectively.

Optical Properties. The doping of yttrium and gadolinium oxidic matrixes with Eu^{III} and Tb^{III} luminescent cations gives them interesting emission properties.[4] For an excitation wavelength within the UV (typically around 260 nm), a charge-transfer process related to the excitation of an electron from the oxygen 2p orbital to the $4f^6$ (Eu^{III}) or $4f^8$ (Tb^{III}) configurations takes place.[4]

A subsequent radiative deexcitation leads to sharp emission in the red and green regions of the visible spectrum. Figure 4a shows the excitation spectrum monitored within the $^7F_2$ manifold of the gadolinium nanohybrids doped with 5% europium. The spectrum presents mainly a broad band centered at 285 nm and a series of low-intensity intra-$4f^6$

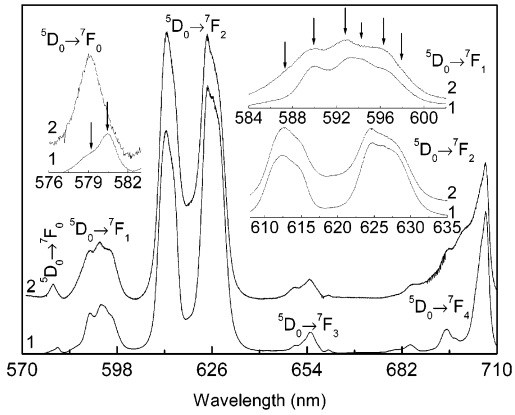

Figure 5. Low-temperature (14 K) emission spectra of gadolinium/europium-based nanohybrid excited at (1) 285 and (2) 395 nm.

lines. This band (285 nm) is red-shifted compared to the one expected for the charge-transfer process related to the excitation of an electron from the 2p oxygen orbital to the $4f^6$ orbital (260 nm).[4] Such band is likely due to the excitation of the phenyl rings of the benzoate molecules between the layers and then further transferred to the Eu^{III} centers. The presence of such a band in the excitation spectrum demonstrates that the benzoate complex plays an important role in the emission characteristic of the nanohybrids. Moreover, this transfer proves that the coordination of the Eu^{III} cations is more complex than in the cubic or monoclinic structure. The excitation spectrum in Figure 4a also displays a lower-intensity band between 350 and 450 nm, whose origin will be discussed in more detail for the Tb^{III}-based nanohybrids.

Figure 4b shows the emission spectra via excitation into the phenyl rings of the benzoate molecules (285 nm) and into the maximum of the lower-intensity excitation band (that coincides with the $^5L_6$ level, 395 nm). For excitation via the benzoate complex, the emission spectrum presents the typical Eu^{III} intra-$4f^6$ $^5D_0 \rightarrow {}^7F_{0-4}$ electronic transitions. No emission arising from the ligands could be detected, reinforcing the energy transfer between the benzoate complex and the Eu^{III} ions. When the nanohybrids are excited at 395 nm, a large broad band is observed between 400 and 700 nm, superimposed on the $^5D_0 \rightarrow {}^7F_{0-4}$ transitions. The changes in the excitation wavelength induce variations in the number, energy, and full width at half-maximum of the components of the $^5D_0 \rightarrow {}^7F_{0-4}$ transitions. To get further insight into the Eu^{III} local coordination, higher-resolution spectra were scanned for Eu^{III} intra-$4f^6$ levels (395 nm) and indirect excitation via benzoate molecules (285 nm) at low temperature. As Figure 5 evidences, there are two clearly components for the nondegenerated $^5D_0 \rightarrow {}^7F_0$ line. Furthermore, the $^5D_0 \rightarrow {}^7F_1$ transition presents at least 5 Starks components; the maximum splitting allowed for a single Eu^{III} local environment is 3 ($2J + 1$). These observations clearly point out the presence of more than one local Eu^{III} site. By comparison of the $^5D_0 \rightarrow {}^7F_{0-4}$ emissions with the data available,[22] the emissions observed agree well with the europium diluted in the Ln_2O_3-type monoclinic structure. However in the present case the oxide layers composing the nanohybrids are so thin (~0.6 nm) that almost all the europium atoms should be present at the surface, and thus they are coordinated to the benzoate molecules. Hence, the $^5D_0 \rightarrow {}^7F_{0-4}$ emission lines reflect the complex local structure of the Eu^{III} cations that in fact consists of two different coordinations: a classical oxidic one (Eu−O−Ln) and a benzoate bridged-like complex (Eu−O−C). Since the relative contribution of the two $^5D_0 \rightarrow {}^7F_0$ emission lines depends on the excitation path, the low-energy component is attributed to Eu^{III} atoms that are in contact with the surface of the oxide layer and hence preferentially excited via the benzoate molecules.

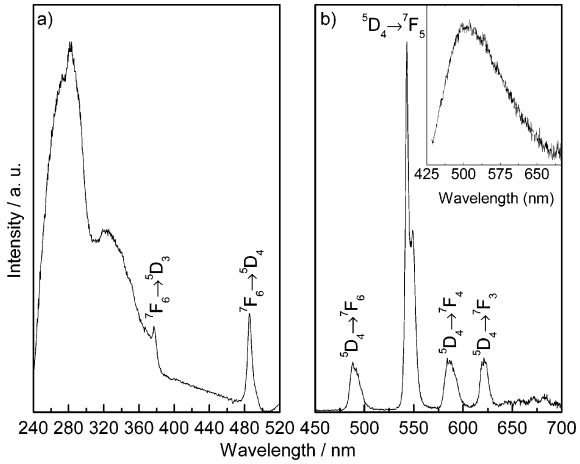

Figure 6. Room-temperature (a) excitation and (b) emission spectra of gadolinium/terbium-based nanohybrid monitored around 544 nm and excited at 288 nm. (Inset) Room-temperature emission spectrum excited at 420 nm.

The luminescence features of the same oxide doped with terbium instead of europium are presented in Figure 6. The excitation spectrum monitored within the Tb^{III} emission lines is formed of two main bands in the UV at around 285 and 320 nm superimposed on a series of $4f^8$ Tb^{III} straight lines. The UV band may be ascribed to the phenyl rings of the benzoate molecules, similarly to the previous discussion on the Eu^{III}-based nanohybrids. When the hybrids are excited into this UV band or directly into the intra-$4f^8$ levels, the typical Tb^{III} $^5D_4 \rightarrow {}^7F_{6-3}$ transitions in the green part of the visible spectrum are observed (Figure 6b). When the hybrids are excited at 420 nm, a large broad band centered at 550 nm appears and no sign of intra-$4f^8$ lines could be detected. Such emission band may arise from phenyl rings of the benzoate molecules whose emitting levels overlap the Tb^{III} excited states. Thus, the excitation spectrum in Figure 6a shows the excitation contributions of both emissions (Tb^{III} and benzoate molecules).

The emission band arising from phenyl rings of the benzoate molecules is also present in the emission and excitation spectra of the other lanthanide- (Sm^{III} and Nd^{III}) based hybrids, as Figure 7 demonstrates. For the former hybrids no sign of the Sm^{III} intra-$4f^5$ lines could be observed, whereas for the neodymium-based hybrid a series of $4f^3$ self-absorptions and the $^4F_{3/2} \rightarrow {}^4I_{9/2}$ transition are detected. Upon exciting the sample within the $^4F_{3/2}$ manifold, the typical Nd^{III} near-infrared emission (NIR) around 1310 nm was observed, which is the II low-loss window of commercial silica-based transmission fibers used in telecommunications (inset of Figure 7).

The room-temperature excitation spectrum monitored around 800 nm displays the typical energy transfer band in

(22) Bihari, B.; Eilers, H.; Tissue, B. M. *J. Lumin.* **1997**, *75*, 1.

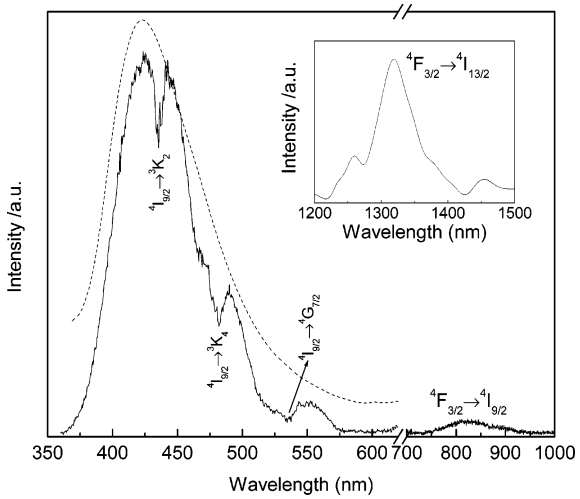

Figure 7. Room-temperature emission spectra of neodymium- (—) and samarium- (•••) based nanohybrids excited at 350 nm. (Inset) Nd^{III} near-infrared emission (excited at 1064 nm).

the UV region and the band ascribed to the phenyl rings of the benzoate molecules (around 420 nm). Those bands are superimposed on intra-$4f^3$ Nd^{III} lines (not shown).

The decay curves of the $^5D_0$ (Eu^{III}), $^5D_4$ (Tb^{III}), and $^4F_{3/2}$ (Nd^{III}) were monitored within the lanthanide-emitting lines at an excitation within the benzoate complex band (around 285 nm). The decay curves for the Nd^{III}-based hybrid were monitored at 14 K (the room-temperature lifetime lies beyond the detection limits of our equipment, $<10^{-6}$ s); whereas for the remaining nanohybrids the lifetime values refer to room-temperature measurements. All the decays curves are well reproduced by a single-exponential function (not shown), revealing lifetime values of 0.640 ± 0.002 ($^5D_0$), 0.848 ± 0.008 ($^5D_4$), and 0.008 ± 0.001 ms ($^4F_{3/2}$). For the gadolinium-based hybrid containing Eu^{III}, the $^5D_0$ decays curves were also monitored under direct excitation into the intra-$4f^6$ levels ($^5L_6$, 395 nm). A smaller $^5D_0$ lifetime was estimated in comparison with those found for excitation via the phenyl rings of the benzoate molecules. The variation of the lifetime values with changes in the excitation wavelength is compatible with the presence of more than one Eu^{III} local environment, as unequivocally pointed out by the luminescence spectra.

From the above luminescence features, the energy transfer mechanisms between the phenyl rings of the benzoate molecules and the lanthanide ions present higher efficiency for the Eu^{III}-based nanohybrids. This conclusion is based on the higher intensity band of the phenyl rings of the benzoate molecules in the excitation spectra of the Eu^{III} hybrids relative to that of the intra-$4f^6$ lines. To quantify the contribution of such energy transfer to the overall luminescence features, the absolute emission quantum yield of the gadolinium-based hybrid containing Eu^{III} was calculated under excitation via the phenyl rings of the benzoate molecules (284 nm). A quantum yield of $16\% \pm 2\%$ was estimated. As observed in many other works dealing with luminescence of nanoparticles or nanostructured materials, the quantum yield is in many cases reduced by defects and hydroxyl groups at the oxide interface. Thus, higher values could probably be achieved if residual crystalline defects and nonradiative relaxations from hydroxyl surface groups are controlled. There are very few results concerning the determination of the absolute quantum yields in lanthanide-based organic/inorganic hybrids. The quantum yield obtained here for the gadolinium-based nanohybrid containing Eu^{III} is similar to the maximum values found for organic/inorganic hybrids incorporating $Eu(CF_3SO_3)_3$ ($13\% \pm 1\%$)[23] and $Eu(nta)_3bpy$ [where nta is 1-(2-naphthyl)-4,4,4-trifluoro-1,3-butanedionate and bpy is 2,2′-bipyridine] ($15.0\% \pm 1.5\%$).[24] Concerning other lanthanide ions, a maximum quantum yield value of 11% for Ce^{3+}-based organic/inorganic hybrids was also reported.[25]

Conclusion

The successful nonaqueous sol−gel reaction between lanthanide alkoxides and benzyl alcohol is shown to be a general route to the formation of organic/inorganic ordered hybrid structures. The synthesis leads to the formation of crystalline thin layers of lanthanide oxides equally spaced by an organic layer formed by benzoate molecules, and the periodic lamellar structure is kept together by simple $\pi-\pi$ interactions between the phenyl rings; surprisingly, the hybrid structures are stable at temperature up to 400 °C.

By doping the gadolinium-based nanohybrids with Eu^{III} and Tb^{III}, it was possible to obtain phosphors showing a strong emission in the red and green part of the visible spectrum, respectively. Since the doped nanohybrids are excited in the organic subphase, where the excitation of the phenyl rings composing the organic layers is effectively transferred to the emitting atoms, the energy needed for the excitation of the luminescent centers is substantially lower than that needed in their corresponding pure inorganic oxides. Furthermore, the intrinsic emission properties of the neodymium-based nanohybrid in the IR are compatible with the requirements of transmission fibers used in telecommunications.

Finally, the general simple route permits one to simply tune the optical properties of the final material just by changing the amount and kind of lanthanide alkoxide.

In a next step the effect of codoping and the modification of the organic layer will be investigated in order to be able to tune more accurately the physical properties (e.g., magnetic, electric, and optical) of these ordered hybrid structures.

Acknowledgment. S. S. Nobre is warmly acknowledged for help with photoluminescence measurements, and Thomas Müller from the University of Halle, for TGA and DTA measurements

Supporting Information Available: TGA and DTA of the nanohybrids under air and argon, FT-IR spectra of the nanohybrids, CHN analysis, and TEM images of the Nd- and Y-based nanohybrids synthesized at 300 °C. This material is available free of charge via the Internet at http://pubs.acs.org.

CM060705L

(23) Sá Ferreira, R. A.; Carlos, L. D.; Gonçalves, R. R.; Ribeiro, S. J. L.; Bermudez, V. de Z. *Chem. Mater*. **2001**, *13*, 2991.
(24) Fu, L.; Sá Ferreira, R. A.; Silva, N. J. O.; Fernandes, J. A.; Ribeiro-Claro, P.; Gonçalves, I. S.; Bermudez, V. de Z.; Carlos, L. D. *J. Mater. Chem.* **2005**, *15*, 3117.
(25) Isakawi, M.; Kuraki, J.; Ito, S. *J. Sol-Gel Sci. Technol.* **1998**, *13*, 587.